Spin-projected unrestricted Hartree-Fock ground states for harmonic quantum dots

U. De Giovannini,[1] F. Cavaliere,[1] R. Cenni,[2] M. Sassetti,[1] and B. Kramer[3]
[1]*Dipartimento di Fisica, Università di Genova, LAMIA CNR-INFM, Via Dodecaneso 33, 16146 Genova, Italy*
[2]*Istituto Nazionale di Fisica Nucleare-Sezione Genova Dipartimento di Fisica, Università di Genova, Via Dodecaneso 33, 16146 Genova, Italy*
[3]*I. Institut für Theoretische Physik, Universität Hamburg, Jungiusstraße 9 20355 Hamburg, and Jacobs University Bremen, Campus Ring 1, 28759 Bremen, Germany*
(Received 24 July 2007; published 22 January 2008)

We report the results for the ground state energies and wave functions obtained by projecting spatially unrestricted Hartree-Fock states to eigenstates of the total spin and the angular momentum for harmonic quantum dots with $N \leqslant 12$ interacting electrons including a magnetic field. The ground states with the correct spatial and spin symmetries have lower energies than those obtained by the unrestricted method. The chemical potential as a function of a perpendicular magnetic field is obtained. Signature of an intrinsic spin blockade effect is found.

DOI: 10.1103/PhysRevB.77.035325 PACS number(s): 73.23.Hk, 73.63.Kv

I. INTRODUCTION

Systems such as atoms, metal clusters, trapped bosons, and quantum dots show several universal features.[1] For example, strongly interacting electrons in quantum dots arrange themselves in a rotating Wigner molecule.[2–5] Rotating boson molecules have been predicted to exist in ion traps.[6] Furthermore, symmetric potentials can induce a shell structure in atoms,[7] metal clusters,[8] and quantum dots.[9] In the latter, signatures of the shell structure have been experimentally probed,[10,11] leading to Hund's rules for the total spin of the electron ground state. The spin in quantum dots[12] also affects the electron transport. It can lead to spin blockade[13,14] and negative differential conductance in nonlinear transport,[13,15–18] and it induces periodic modulations of the positions of the Coulomb peaks in the linear conductance as a function of an applied magnetic field.[16,19–21] Recently, the spatial distribution of spin in the Kondo effect has been probed.[22–25]

Studying the ground state properties of quantum dots, also in the presence of a magnetic field B, mean field methods such as Hartree-Fock (HF)[3,26–31] and the density functional theory[32–38] have been used. These are often believed not to provide the most accurate estimates for the ground state energies and even to produce unphysical symmetry breakings due to incomplete ansatz wave functions. For instance, neglecting correlations, the straightforward HF method starts from a single Slater determinant as a variational many-body wave function which not necessarily is an eigenstate of the total spin.[39] Spatially unrestricted Hartree-Fock (UHF)[3,27] methods systematically use symmetry breaking in order to obtain better estimates for the ground state energy. This may lead to wrong results for the total angular momentum and the total spin. For instance, UHF calculations sometimes seem to fail predicting the total spin resulting from Hund's rule, in contradiction to the more accurate methods. Violations of Hund's rules for relatively weak Coulomb interactions have been reported[3] for $N=4,8,9$.

Projection techniques,[40–42] pioneered in the 50th of the last century, can be applied for introducing the correct spatial and spin symmetries. Additionally, the procedure introduces correlations into the ground state wave function that are absent in a single UHF Slater determinant. For quantum dots, they first have been used for obtaining wave functions corresponding to specific angular momenta.[43–47] Restoring the *spin* symmetry has received comparatively less attention, and it has been used for small N.[43,48–50] In view of the recent discussion of spin effects in the transport spectra of quantum dots with larger N, information about the total spin is necessary.

Recently, the rotational and spin symmetry restorations have also been approached by means of other techniques. The random phase approximation has been used to restore the rotational symmetry of wave functions obtained by UHF.[51] For $N=2$, the spin singlet has also been approximately restored with the Lipkin-Nogami approach.[52]

For small N, exact diagonalization (ED),[4,53–64] configuration interaction (CI),[65,66] and stochastic variational methods[67] allow for precisely determining ground and excited state energies and their quantum numbers. Presently, reliably converged "exact" results can be obtained only for electron numbers up to $N \approx 8$ electrons.[66]

For $N \leqslant 13$, $N=16,24,48$, approximate methods such as quantum Monte Carlo (QMC)[68–76] have been used. They can provide reasonably accurate estimates for ground and excited states energies, giving rise to the shell structure, Hund's rules, Wigner crystallization, and "magic" angular momenta.[2,57,71,73–75,77–79] Results for higher N have been restricted to zero magnetic field.

In this paper, we apply systematically the previously mentioned projection techniques to the states obtained by UHF for estimating the ground state energy of a circular quantum dot with $N \leqslant 12$ electrons, including a magnetic field. Starting from an UHF Slater determinant with broken rotational symmetry, a first estimate for the ground state energy and the wave function is obtained. Then, *both the total spin and the angular momentum* of the UHF variational wave function are introduced. We show that, after restoring *all of the symmetries*, the energies and the wave functions are improved and show physical features which are discarded by the UHF method.

We discuss the efficiency of the projected Hartree-Fock (PHF) method by comparing our results with those of ED, CI, and QMC. We determine the ground state energies as a function of a magnetic field and obtain the chemical potential that can be measured in transport experiments. Our main findings are as follows.

(i) By projecting the UHF wave functions on the total angular momentum L and on the total spin S, the ground state energy is successively lowered. The correction due to the spin projection is generally smaller than the one associated with the angular momentum, but still necessary for determining the correct ground state and its quantum numbers.

(ii) The quantum numbers L and S are correctly reproduced, if the strength of the interaction is not too large. Especially, for $B=0$, the first Hund's rule—namely, that S is maximized for open shells—is recovered for $N\leqslant 12$ electrons, except for $N=10$, discussed below.

(iii) Comparing the results with CI and QMC, we find a correlation energy (difference between PHF and exact energies) of about 2% of the ground state energy.

(iv) With increasing interaction strength, the correlation energy decreases. Nevertheless, for stronger interaction, and larger N, the PHF ground state tends to have $L=0$ with a high total spin. This is reminiscent of the formation of a rigid rotating Wigner molecule.[44]

(v) As a function of B, several crossovers between ground states with different total spins and angular momenta are found that are absent in UHF. These are associated with changes in the electron densities. The onset of the singlet-triplet transition[30] occurring for dot filling factor $\nu\approx 2$ and N even is recovered. Features that lead to an intrinsic spin blockade are predicted.

In the next section, details of the UHF method are outlined. The consequences of the broken symmetries are described and the projection technique is discussed, with special emphasis on the total electron spin. In Sec. III, results for zero and nonzero magnetic fields are presented and discussed.

II. MODEL AND METHOD

A. Model

Consider N electrons in a two-dimensional (2D) quantum dot confined by an in-plane harmonic potential and subjected to a perpendicular magnetic field $\mathbf{B}=B\mathbf{e}_z$. The Hamiltonian ($\hbar=c=1$)

$$H=\sum_{i=1}^{N} h_0(\mathbf{r}_i,s_{zi})+\frac{1}{2}\sum_{\substack{i,j=1\\ i\neq j}}^{N} v(\mathbf{r}_i-\mathbf{r}_j), \tag{1}$$

with

$$h_0(\mathbf{r},s_z)=\frac{[\mathbf{p}+e\mathbf{A}(\mathbf{r})]^2}{2m^*}+\frac{m^*\omega_0^2}{2}\mathbf{r}^2+g^*\mu_B B s_z, \tag{2}$$

$\mathbf{r}\equiv(r,\vartheta)$ the 2D polar coordinates, $v(\mathbf{r})=e^2/4\pi\varepsilon_0\varepsilon_r r$ the Coulomb interaction potential, $\mathbf{B}=\mathrm{rot}\mathbf{A}$, m^* effective electron mass, ω_0 confinement frequency, g^* effective g factor, and μ_B the Bohr magneton. The z component of the ith spin is $s_{zi}=\pm 1/2$, $-e$ the electron charge, and ε_r the relative dielectric constant. The term $h_0(\mathbf{r},s_z)$ in Eq. (1) yields the Fock-Darwin[80] (FD) spectrum,

$$\epsilon_{n,l,s_z}=\Omega(2n+|l|+1)+\frac{\omega_c}{2}l+g^*\mu_B B s_z, \tag{3}$$

where we have introduced the effective confinement frequency $\Omega=(\omega_0^2+\omega_c^2/4)^{1/2}$ with $\omega_c=eB/m^*$ the cyclotron frequency. The eigenfunctions are $\phi_{n,l}(\mathbf{r})\chi^{\pm}$, where $\chi^{\pm}$ is the spinor corresponding to $s_z=1/2$ ($s_z=-1/2$) and $\phi_{n,l}(\mathbf{r})$ are given in Ref. 80. Here, n and l are the principal and angular momentum quantum numbers. At $B=0$, expressing energies in units ω_0 and lengths in units $\ell_0=(m^*\omega_0)^{-1/2}$, the Hamiltonian (1) depends only on the dimensionless interaction strength,

$$\lambda=\frac{e^2}{4\pi\varepsilon_0\varepsilon_r\ell_0\omega_0}. \tag{4}$$

B. Unrestricted Hartree-Fock method

In HF, the Schrödinger equation for a given value of total $S_z=s_{z1}+\cdots+s_{zN}$ is solved by using orbitals

$$\psi_i^{\alpha}(\mathbf{r})=u_i^{\alpha}(\mathbf{r})\chi^{\alpha},\quad 1\leqslant i\leqslant N_{\alpha}, \tag{5}$$

with $\alpha=+$ ($\alpha=-$) denoting spin up (down) and N_{α} the number of electrons with spin $\alpha 1/2$. They are obtained as the self-consistent solutions of coupled integrodifferential equations starting from an initial guess.[39,42] The many-body wave function is a single Slater determinant $|\Psi^{S_z}\rangle$, eigenfunction of S_z, which corresponds to a stationary point of the UHF energy,[39,42]

$$E^{S_z}=\frac{\langle\Psi^{S_z}|H|\Psi^{S_z}\rangle}{\langle\Psi^{S_z}|\Psi^{S_z}\rangle}. \tag{6}$$

It is convenient to expand the orbitals $\psi_i^{\alpha}(\mathbf{r})$ in the FD basis $\phi_{\mu}(\mathbf{r})\chi^{\alpha}$,

$$\psi_i^{\alpha}(\mathbf{r})=\sum_{\mu=1}^{K} C_{\mu i}^{\alpha}\phi_{\mu}(\mathbf{r})\chi^{\alpha},\quad 1\leqslant\mu\leqslant K, \tag{7}$$

where $C_{\mu i}^{\alpha}$ are complex coefficients. The truncation of the basis to K states is needed to numerically implement the procedure. We have used the $K=75$ lowest FD states for each value of B (see Sec. II D). Introducing the density matrices,

$$P_{\mu\nu}^{\alpha}=\sum_{i=1}^{N_{\alpha}} C_{\mu i}^{\alpha}(C_{\nu i}^{\alpha})^*, \tag{8}$$

the HF problem can be cast into the numerically suitable coupled nonlinear Pople-Nesbet eigenvalue problem,[39]

$$\sum_{\nu=1}^{K} F_{\mu\nu}^{\alpha} C_{\nu i}^{\alpha} = \varepsilon_i^{\alpha} C_{\mu i}^{\alpha}. \tag{9}$$

Here, $F_{\mu\nu}^{\alpha}$ are the Fock matrices,

$$F_{\mu\nu}^{\alpha} = \epsilon_{n_\mu, l_\mu, \alpha 1/2} \delta_{\mu\nu} + \sum_{\lambda,\eta=1}^{K} P_{\lambda\eta}^{\alpha} [v_{\mu\eta\nu\lambda} - v_{\mu\eta\lambda\nu}] + P_{\lambda\eta}^{-\alpha} v_{\mu\eta\nu\lambda},$$

with the two-body interaction matrix elements[66]

$$v_{\mu\eta\nu\lambda} = \int d\mathbf{r}_1 d\mathbf{r}_2 \phi_\mu^*(\mathbf{r}_1) \phi_\eta^*(\mathbf{r}_2) v(\mathbf{r}_1 - \mathbf{r}_2) \phi_\nu(\mathbf{r}_1) \phi_\lambda(\mathbf{r}_2).$$

The energy [Eq. (6)] is then

$$E^{S_z} = \frac{1}{2} \sum_{\alpha=\pm} \sum_{\mu,\nu=1}^{K} [\epsilon_{n_\nu, l_\nu, \alpha 1/2} \delta_{\nu\mu} + F_{\nu\mu}^{\alpha}] P_{\mu\nu}^{\alpha}. \tag{10}$$

We use *spatially unrestricted* initial conditions[3,27,43] with a random distribution of initial $C_{\mu,\nu}^{\alpha}$. This implies initial orbitals without circular symmetry, and it leads to better energy estimates. However, symmetry broken Slater determinants are, in general, neither eigenfunctions of the total angular momentum $L=l_1+\cdots+l_N$ nor of $\mathbf{S}^2$ (total spin $\mathbf{S}=\mathbf{s}_1+\cdots+\mathbf{s}_N$).[39]

The most general UHF solution is a linear superposition of eigenfunctions $|\Psi^{S_z}(L,S)\rangle$ of L and $\mathbf{S}^2$,

$$|\Psi^{S_z}\rangle = \sum_{L=-\infty}^{\infty} \sum_{S \geq |S_z|}^{N/2} |\Psi^{S_z}(L,S)\rangle. \tag{11}$$

For given N and S_z, many initial conditions are used. Correspondingly, several stationary points are found. They form a sequence $|\Psi_k^{S_z}\rangle$ $(k=1,2,\cdots)$ with energies $E_1^{S_z} < E_2^{S_z} < \ldots$. For a given S_z, the process is iterated until the lowest $E_1^{S_z}$ is found. The UHF ground state is defined as

$$E_{\mathrm{UHF}} = \min_{S_z} \{E_1^{S_z}\}.$$

C. Spin and angular momentum projection

In order to obtain states with specific L and S, we act on the UHF Slater determinant with operators[42] $\hat{P}_L$ and $\hat{P}_S^{S_z}$ which project on $\hat{L}$ and $\hat{\mathbf{S}}$, respectively (to avoid confusion, in this section, operators are denoted by an overhat). They satisfy commutation rules $[\hat{P}_S^{S_z}, \hat{P}_L] = [\hat{P}_S^{S_z}, \hat{H}] = [\hat{P}_L, \hat{H}] = 0$. Their action yields an eigenfunction of $\hat{L}$ and $\hat{\mathbf{S}}^2$,

$$\hat{P}_L \hat{P}_S^{S_z} |\Psi^{S_z}\rangle = |\Psi^{S_z}(L,S)\rangle.$$

The corresponding energy[50]

$$E^{S_z}(L,S) = \frac{\langle \Psi^{S_z} | \hat{H} | \Psi^{S_z}(L,S) \rangle}{\langle \Psi^{S_z} | \Psi^{S_z}(L,S) \rangle}. \tag{12}$$

The spin projector,

$$\hat{P}_S^{S_z} = \prod_{k=|S_z|, k\neq S}^{N/2} \frac{\hat{S}^2 - k(k+1)}{S(S+1) - k(k+1)}, \tag{13}$$

annihilates the components of $|\Psi^{S_z}\rangle$ with spin different from S.[40,48,49] Its action can be written as[40,81] $\hat{P}_S^{S_z} |\Psi^{S_z}\rangle = \sum_{q=0}^{N_<} C_q(S,S_z,N) |T_q\rangle$, where $N_< = \min\{N_+, N_-\}$ and $C_q(S,S_z,N)$ are the Sanibel coefficients.[50,81,82] The term $|T_q\rangle = |T_q^{(1)}\rangle + \cdots + |T_q^{(n_q)}\rangle$ is the sum of all $n_q = \binom{N_+}{q}\binom{N_-}{q}$ Slater determinants obtained by swapping, without repetition, *all* the possible q spinor pairs with opposite spins in $|\Psi^{S_z}\rangle \equiv |T_0\rangle$.

The projector on $\hat{L}$ is given by[42]

$$\hat{P}_L = \frac{1}{2\pi} \int_0^{2\pi} d\gamma e^{-iL\gamma} e^{i\hat{L}\gamma}, \tag{14}$$

where $\exp(i\hat{L}\gamma)$ acts on $|T_q\rangle$ rotating by γ all spatial parts of the orbitals: $u_i^{\alpha}(r,\vartheta) \to u_i^{\alpha}(r,\vartheta+\gamma)$. We denote this by $|T_q(\gamma)\rangle$. Combining the expressions for spin and angular momentum projectors, we can finally calculate $|\Psi^{S_z}(L,S)\rangle$. It is a sum of many Slater determinants. This indicates that correlation has been introduced by the projection. Further details concerning the projection techniques are provided in Appendix.

The main computational effort is due to the evaluation of two-body matrix elements in Eq. (12). The projection of an N-particle UHF state with S_z to a state with total spin S needs $n(S_z,N) = \sum_{q=0}^{N_<} n_q = \binom{N}{S_z+N/2}$ terms. For N even (odd), the worst case is $S_z=0$ $(S_z=1/2)$.

For the angular momentum projection, we use a fast Fourier transform (FFT) and partition the integration interval $[0,2\pi]$ in $n(L)$ points; $n(L)$ is determined by the angular momentum range $|L| \leq L_{max}$ for which good convergence (relative error of $<10^{-6}$) of the PHF energies is required. We have checked that for $L_{max}=20$, used throughout the paper, $n(L)=256$ is needed. Using FFT, all energy values for given S and $|L| \leq L_{\max}$ are *simultaneously* available, which considerably accelerates the calculation with respect to performing distinct computations for each value of L. The total number of two-body matrix elements is $n_{tot} = n(S_z,N)n(L)$. Although n_{tot} quickly increases as a function of N, especially because $n(S_z,N)$ grows exponentially for large N, it still compares favorably with respect to exact methods. For example, previously reported ED calculations[61] used a basis of 19 774 Slater determinants for $N=4$, $S_z=0$, $S=2$, and $L=14$. CI calculations[66] for $N=6$, $S_z=0$, $S=0$, and $L=0$ need 661 300 configurational state functions (linear superposition of Slater determinants). For these values, PHF requires the evaluation of 1536 and 5120 matrix elements, respectively.

To determine the ground state, it is generally *not* sufficient to project only the UHF ground state. If several UHF solutions (Sec. II B) are almost degenerate, all of the $|\Psi_i^{S_z}\rangle$ have to be projected giving $|\Psi_i^{S_z}(L,S)\rangle$. The PHF ground state is then defined by

$$E_{\mathrm{PHF}} = \min_{\{i,S_z,L,S\}} \{E_i^{S_z}(L,S)\}. \quad (15)$$

One can show that projecting arbitrary UHF Slater determinants on L and S always leads to energies that are *not lower* than the exact ground state energy, thus satisfying the variational principle. The determination of the PHF ground state is illustrated in detail in Ref. 50.

D. Some comments about errors

The major systematic error of the UHF method is to neglect correlations. By projecting the Slater determinant on fixed angular momentum and spin PHF attempts to correct for these effects. A second systematic effect is due to the uncertainty if the self-consistent HF procedure has converged to the absolute energy minimum.

For getting insight into these systematic effects, one can start from wave functions with the same L,S but originating from UHF states with different S_z. They should be degenerated at $B=0$. As an example, we consider $N=4$ for $B=0$, with confinement energy $\omega_0=0.741$ meV. We assume the standard GaAs parameters, $m^*=0.067m_e$ and $\varepsilon_r=12.4$, corresponding to $\lambda=4$. The states $|\Psi_1^0(1,1)\rangle$ [with $E_1^0(1,1)=19.404\omega_0$] and $|\Psi_1^1(1,1)\rangle$ [with $E_1^1(1,1)=19.394\omega_0$] should have the same energy. The same for $|\Psi_2^0(0,1)\rangle$ [energy $E_2^0(0,1)=19.331\omega_0$] and $|\Psi_1^1(0,1)\rangle$ [energy $E_1^1(0,1)=19.342\omega_0$]. Their energetic differences of $0.010\omega_0$ and $0.011\omega_0$, respectively, correspond to a relative uncertainty of 5×10^{-4}. Similar estimates for the "degeneracy error" is obtained from data for different N and λ (see, for example Table 2). We attribute the degeneracy error mainly to UHF: different UHF states in different S_z sectors approximate the true states with different precisions. Therefore, their projection on the same L,S sector does not yield exactly degenerate states.

Also, the convergence with respect to the FD basis size K has been studied. In determining the UHF ground state energies, we found that with $K=100$, the relative energy improvement with respect to $K=75$ case is less than 10^{-6}. We therefore employed $K=75$.

When several PHF energies $E_i^{S_z}(L,S)$ are almost degenerate, one can improve further the ground state: linear superposition of the almost degenerate states $|\Psi_i^{S_z}(L,S)\rangle$ may result in further lowering of the energy. Here, we have not systematically investigated this effect.

III. RESULTS

A. Zero magnetic field

1. Ground state energies

Table I summarizes our results for the ground state energies at $B=0$ for $N\leqslant12$ and $\lambda=1.89,2,4$. Results obtained with diffusion Monte Carlo (DMC)[68,74] and CI[66] are included.

For $\lambda\leqslant2$, angular momenta and total spins of the ground states obtained by PHF agree with DMC and CI. The total spin fulfills Hund's first rule: a singlet state for the filled shells ($N=2,6,12$), a triplet for $N=4$, 8, and $S=3/2$ for $N=9$. Only for $N=10$, Hund's rule is not fulfilled since we find $S=0$ instead of $S=1$. However, here, the degeneracy error is $0.064\omega_0$, larger than the energy distance $\Delta E=0.038\omega_0$ between the ground and the first excited state. Also DMC[68] predicts an extremely small energy gap between the singlet and the triplet, though it yields an $S=1$ ground state.

Increasing the interaction strength ($\lambda=4$), PHF still produces energies consistent with CI and DMC. However, for $N=3,6,7,8$, different quantum numbers for the ground state are predicted with a tendency toward a state with $L=0$ and polarized spin.

For $4<\lambda\leqslant8$, preliminary results (not shown) indicate a similar behavior. Two features are observed: first, the PHF solutions have $L=0$, second they have a high total spin. The tendency toward $L=0$ for strong Coulomb interactions was already discussed in Refs. 4 and 44 within an UHF approach with subsequent projection on the angular momenta. It is reminiscent of the formation of a rigid rotating Wigner molecule characterized by a rotational spectrum $\propto L^2$ at $B=0$, which would then favor $L=0$.

In this respect, the case $N=3$ is peculiar. Here, increasing λ, we find a transition $L=1$, $S=1/2\rightarrow L=0$, $S=3/2$ at $\lambda=2.2$. This is qualitatively similar to ED calculations,[5] where indeed a transition from $L=1$ to $L=0$ is obtained for $\lambda=4.343$. Only the threshold in λ for PHF crossover is smaller than the one for ED.

Current CI and DMC calculations do not display transitions of this kind in the $4\leqslant N\leqslant8$ and $\lambda\leqslant8$ range we explored, with the possible exception of the DMC calculation of Ref. 74 which reports $L=0,S=1/2$ for the ground state of $N=7$ at $\lambda=8$ (for $\lambda=2,4$, CI and DMC predict $L=2$). It is also possible that the HF tendency to overestimating the exchange as compared to correlations may contribute to shift the crossover threshold to smaller λ.

The relative deviation $\delta=(E_{\mathrm{PHF}}-E_{\mathrm{DMC}})/E_{\mathrm{DMC}}$ for[68] $\lambda=1.89$ and $2\leqslant N\leqslant12$ is shown in Fig. 1; δ is largest for the closed shells $N=2,6,12$. Except for $N=2$, $\delta\approx2\%$. The inset shows δ for $N=2$ (squares with $L,S=0,0$), $N=4$ (dots with $L,S=0,1$), and $N=6$ (triangles with $L,S=0,0$) within $1.89\leqslant\lambda\leqslant8$. A decrease with λ according to a power law is ob-

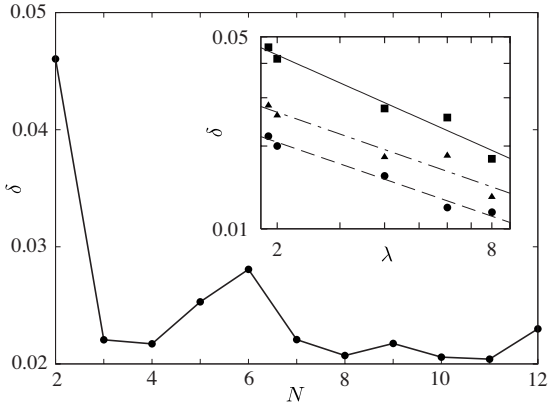

FIG. 1. Deviations δ between PHF and DMC (Ref. 68) for $2\leqslant N\leqslant12$, with $\lambda=1.89$ (Table I). Inset: double logarithmic plot of $\delta(\lambda)$ from PHF and QMC (Ref. 68) ($\lambda=1.89$) and QMC (Ref. 74) and CI (Ref. 66) ($\lambda\geqslant2$) for $N=2$ (squares), $N=4$ (dots), and $N=6$ (triangles). Lines: best fits to data.

TABLE I. Ground state energies from PHF for $N \leqslant 12$ and $\lambda = 1.89, 2, 4$ with corresponding L, S ($m^* = 0.067 m_e$ and $\varepsilon_r = 12.4$) together with results from CI (Ref. 66) and DMC (Ref. 68 for $\lambda = 1.89$, Ref. 74 for $\lambda \geqslant 2$). All energies are in units ω_0.

N	λ	E_{PHF}	L S	E_{CI}	E_{DMC}	L S
2	1.89	3.817	0 0		3.649	0 0
	2	3.885	0 0	3.7295		0 0
	4	4.983	0 0	4.8502		0 0
3	1.89	8.154	1 1/2		7.978	1 1/2
	2	8.337	1 1/2	8.1671		1 1/2
	4	11.131	0 3/2	11.043		1 1/2
4	1.89	13.554	0 1		13.266	0 1
	2	13.899	0 1	13.626		0 1
	4	19.330	0 1	19.035		0 1
5	1.89	20.264	1 1/2		19.764	1 1/2
	2	20.811	1 1/2	20.33		1 1/2
	4	29.501	1 1/2	28.94		1 1/2
6	1.89	27.905	0 0		27.143	0 0
	2	28.703	0 0	27.98		0 0
	4	41.187	0 3	40.45		0 0
7	1.89	36.627	2 1/2		35.836	2 1/2
	2	37.698	2 1/2			
	4	54.497	0 5/2	(54.68)	53.726	(2)2 (1/2)1/2
8	1.89	46.260	0 1		45.321	0 1
	2	47.659	0 1	47.14	46.679	0 1
	4	69.479	0 4	70.48		0 1
9	1.89	56.853	0 3/2		55.643	0 3/2
10	1.89	68.245	0 0		66.8785	2 1
		(68.283)	2 1		(66.8789)	0 0
11	1.89	80.444	0 1/2		78.835	0 1/2
12	1.89	93.661	0 0		91.556	0 0

served, $\lambda^{-\beta(N)}$. By numerically fitting the data, one finds $\beta(2) = 0.57$, $\beta(4) = 0.44$, and $\beta(6) = 0.45$.

Table II and Fig. 2 illustrate the effect of angular momentum projection alone followed by spin projection for $N=8$ starting with UHF states with $S_z = 0, \ldots, 3$. The energy $E_i^{S_z}(L)$ projected on angular momentum is $E_i^{S_z}(L) = \langle \Psi_i^{S_z} | H | \Psi_i^{S_z}(L) \rangle / \langle \Psi_i^{S_z} | \Psi_i^{S_z}(L) \rangle$, where $|\Psi_i^{S_z}(L)\rangle = P_L |\Psi_i^{S_z}\rangle$. Only the lowest energies are included in the table.

The typical energy gain obtained by angular momentum projection is about $0.25\omega_0$. The spin projection induces corrections of the same order of magnitude, which can even change the sequence of energies (Fig. 2). From the UHF state with $S_z = 0$ and $E_1^0 = 48.150\omega_0$, which is not the UHF ground state, projection on $L=0$ yields $E_1^0(L=0) = 47.842\omega_0$. After projection on the total spin, we obtain the energy of the ground state $E_1^0(L, S=0,1) = 47.659\omega_0$ and an excited state at $E_1^0(L, S=0,2) = 48.031\omega_0$. On the other hand, the energetically lowest UHF minimum $E_1^1 = 48.131\omega_0$ yields the first excited PHF state at $E_1^1(L, S=2,1) = 47.742\omega_0$.

Thus, PHF not only introduces a lowering of the energies but can also restore the correct ordering of energy levels. This can be seen from the last column of Table II, which contains the results obtained by DMC.[74] Restoring the spin plays a crucial role in obtaining *all* correct quantum numbers for the ground state including Hund's rule.[50] For example, with angular momentum projection alone, one would have predicted $L=2$ for the ground state, in contrast to the correct result.

The degeneracy error for this case is approximately $0.06\omega_0$ (some example of almost degenerate states are included in Table II). The distance between ground state and the first excited state is $\approx 0.08\omega_0$. This suggests that the ground state for $N=8$ has $L, S = 0, 1$, consistent with DMC. Even the quantum numbers of the first three excited states

TABLE II. Comparison of the lowest energies $E_i^{S_z}$ obtained from UHF, followed by projection on angular momentum $E_i^{S_z}(L)$, and total spin $E_i^{S_z}(L,S)$ for $N=8$ and $\lambda=2$ ($m^*=0.067m_e$, $\varepsilon_r=12.4$). Last column: energies from DMC (Ref. 74). The ground state has $L,S=0,1$. Superscripts ^{0,1,2,3,4} denote "degenerated" energies with the same quantum numbers L, S but originating from different S_z. All energies are in units ω_0.

$E_i^{S_z}$	S_z	$E_i^{S_z}(L)$	L	$E_i^{S_z}(L,S)$	S	E_{DMC}
48.150	0	47.842	0	47.659^0	1	46.679
			0	48.031^1	2	
		48.088	2	47.790	0	46.875
			2	47.799^4	1	
		47.971	1	47.817^2	2	46.917
			1	48.028^3	1	
		48.076	4	47.777	0	46.779
48.237	0	47.981	0	47.805	0	46.807
		48.025	1	47.910^3	1	
48.131	1	47.796	2	47.742^4	1	46.756
		47.887	1	47.806^2	2	46.917
			1	47.985^3	1	
		48.022	0	47.977^1	2	47.406
			0	47.997^0	1	
48.243	2	47.896	1	47.881^2	2	
48.335	3	48.129	3	48.126	3	47.404

turn out to be reproduced correctly while the fourth and the fifth appear to be interchanged.

2. Ground state densities

For the spin-resolved densities

$$\rho_{\mathrm{PHF}}^{\alpha}(r)=\frac{\langle\Psi^{S_z}(L,S)|\sum_{i=1}^{N_\alpha}\delta(\mathbf{r}-\mathbf{r}_i)\delta_{s_{zi},\alpha 1/2}|\Psi^{S_z}(L,S)\rangle}{\langle\Psi^{S_z}(L,S)|\Psi^{S_z}(L,S)\rangle},$$

we first consider $N=3$ and $N=4$ (Figs. 3 and 4) for intermediate ($\lambda=2$) and strong ($\lambda=8$) interactions. Increasing the interaction strength leads to a shift of the maximum of the densities toward higher r, consistent with earlier findings by ED.[5,57] This is clearly observed in the spin-up density for $N=3$ (Fig. 3). For $N=4$, the ground state ($L=0$, $S=1$, $S_z=0$) densities $\rho_{\mathrm{PHF}}^{+}(r)=\rho_{\mathrm{PHF}}^{-}(r)$ (Fig. 4) agree very well with ED[57] for large r. Generally, deviations occur near $r\approx 0$.

Figure 5(a) shows the total electron density for $N=5$, $L,S=1,1/2$ for $\lambda=0.5,2,10$. For weak interaction, $\lambda=0.5$ (solid line), we find good agreement with CI[83] (squares). For $\lambda=2$ (dashed), small deviations near $r=0$ are found. Figure 5(b) indicates that the spin-down density is responsible for the small deviation from the exact result around $r=0$ for $\lambda=2$.

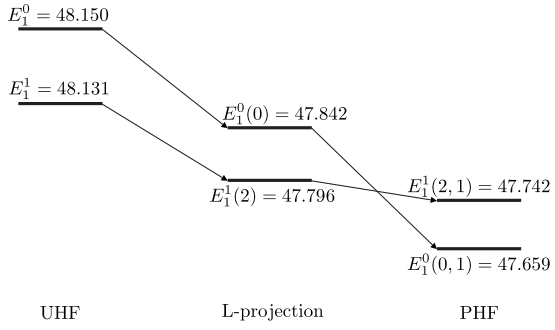

FIG. 2. Influence of the projection procedure on the energy levels (unit ω_0) for $N=8$ and $\lambda=2$. Only the two lowest UHF states (left) directly involved in the determination of the PHF ground state (right) are shown.

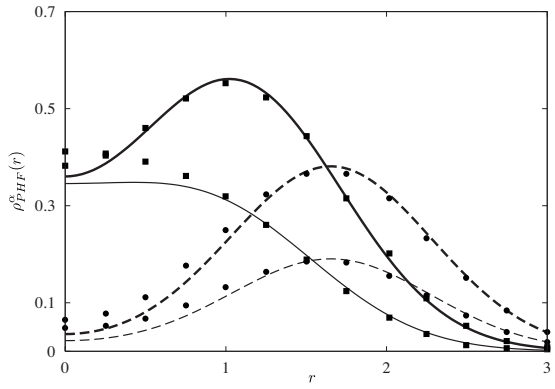

FIG. 3. Spin-resolved densities $\rho_{\mathrm{PHF}}^{\alpha}(r)$ (thick line: $\alpha=+$; thin line: $\alpha=-$) for a GaAs quantum dot with $N=3$, $L=1$, $S=1/2$, and $S_z=1/2$ for interaction strengths $\lambda=2$ (solid) and $\lambda=8$ (dashed). Density unit: $\pi^{-1}\ell_0^{-2}$. Data from ED (Ref. 5): squares $\lambda=2$ and circles $\lambda=8$.

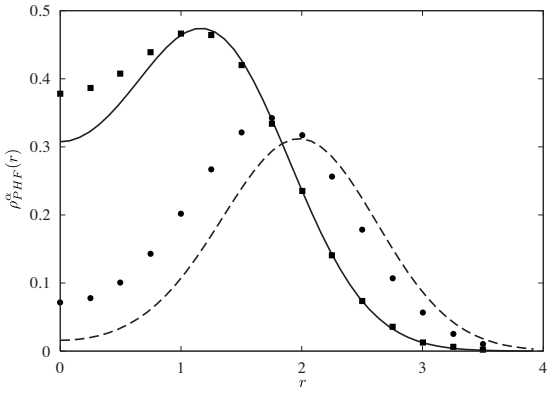

FIG. 4. Spin-resolved densities $\rho^{+}_{\mathrm{PHF}}(r)=\rho^{-}_{\mathrm{PHF}}(r)$ for a GaAs quantum dot with $N=4$, $L=1$, $S=1$, and $S_z=0$ for $\lambda=2$ (solid line) and $\lambda=8$ (dashed line). Density unit: $\pi^{-1}\ell_0^{-2}$. Data from ED (Ref. 57): squares $\lambda=2$ and circles $\lambda=8$.

B. Finite magnetic field

In this section, we show results for $N=5,6,7$ with a magnetic field, $B\leqslant 2.4$ T, corresponding to a dot filling factor $\nu\gtrsim 2$ ($N\leqslant 4$ has been discussed in Ref. 50). We assume here a confinement $\omega_0=6$ meV (corresponding to $\lambda=1.45$) and $g^{*}=-0.44$. For $B>0$, due to the Zeeman term, the PHF ground state always has $S_z=S$. Therefore, we do not specify S_z in the following.

We start with $N=5$ (Fig. 6) and $N=6$ (Fig. 7). We show the UHF ground state energy E_{UHF} (solid line), the energy obtained from angular momentum projection (dashed), and the PHF energy [dashed dotted, Eq. (15)]. The highest energy gain is here due to the angular momentum projection. Spin projection leads to a further decrease of the ground state energy. The UHF and PHF results behave completely differently with B. For instance, for $N=5$ (Fig. 6), the UHF ground state shows crossovers $S_z=1/2\rightarrow 3/2$ at $B\approx 0.9$ T and $S_z=3/2\rightarrow 1/2$ at $B\approx 1.5$ T. In contrast, the PHF energy has total spin $S=1/2=S_z$ in the entire magnetic field region. The

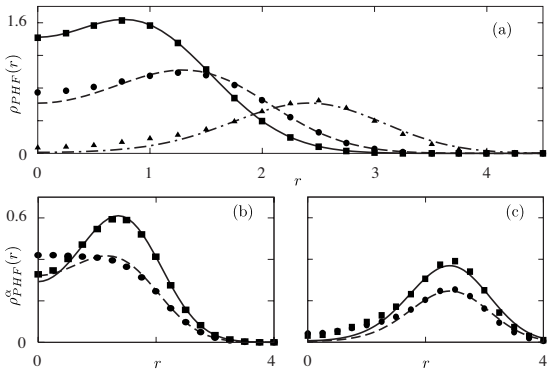

FIG. 5. Densities for $N=5$, $L=1$, $S=1/2$, and $S_z=1/2$. (a) Total density $\rho_{\mathrm{PHF}}(r)=\rho^{+}_{\mathrm{PHF}}(r)+\rho^{-}_{\mathrm{PHF}}(r)$ (units $\pi^{-1}\ell_0^{-2}$) for $\lambda=0.5$ (solid), $\lambda=2$ (dashed), and $\lambda=10$ (dashed dotted). Squares, circles, and triangles: data from CI (Ref. 83). (b) Spin-resolved densities $\rho^{\alpha}_{\mathrm{PHF}}(r)$ (solid: $\alpha=+$, dashed: $\alpha=-$, units $\pi^{-1}\ell_0^{-2}$) for $\lambda=2$. Squares and circles: data from CI (Ref. 83). (c) Same as (b) but $\lambda=10$.

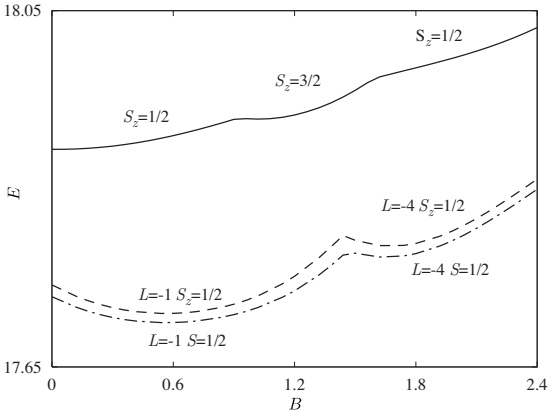

FIG. 6. Ground state energy E (units ω_0) as a function of magnetic field B (units T) for $N=5$. Solid: UHF; dashed: angular momentum projection; dashed dotted: PHF. Here and in the following figures, $m^{*}=0.067m_e$, $\varepsilon_r=12.4$, $g^{*}=-0.44$, and $\omega_0=6$ meV.

state with $S_z=3/2$, not compatible with the total spin $S=1/2$, is certainly an artifact of UHF. The crossover $L,S=1,1/2\rightarrow L,S=4,1/2$ with increasing magnetic field at $B=1.4$ T agrees quantitatively with the earlier results obtained by ED.[84]

For $N=6$ (Fig. 7), UHF (solid line) displays no S_z transitions. When rotational symmetry is restored, two crossovers, *(a)* $L=0\rightarrow -3$ and *(b)* $L=-3\rightarrow -6$, appear. Performing the spin projection, singlet states corresponding to $L=0$ and $L=-6$ are found, and $S=1$ for $L=-3$ is obtained. Singlets have the largest energy gain, leading to a shift of the features found with angular momentum projection (Fig. 7). Also here, the PHF quantum numbers agree with the earlier results obtained by ED,[84] including the magnitudes of the crossover fields at $B\approx 1$ T and $B\approx 1.8$ T, respectively.

The singlet-triplet crossover occurring for $N=6$ at $B\approx 1.8$ T corresponds to a filling factor $\nu\approx 2$, and it is a peculiar feature which is confirmed by several experimental and theoretical studies.[20,21,30,85] Also, for $N=8$, preliminary data indicate such a crossover near $\nu=2$. These crossovers are completely absent in UHF (Fig. 7).

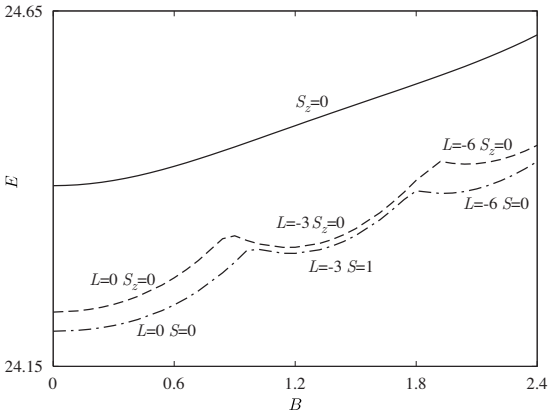

FIG. 7. Ground state energy E (units ω_0) as a function of magnetic field B (units T) for $N=6$. Solid: UHF; dashed: angular momentum projection; dashed dotted: PHF.

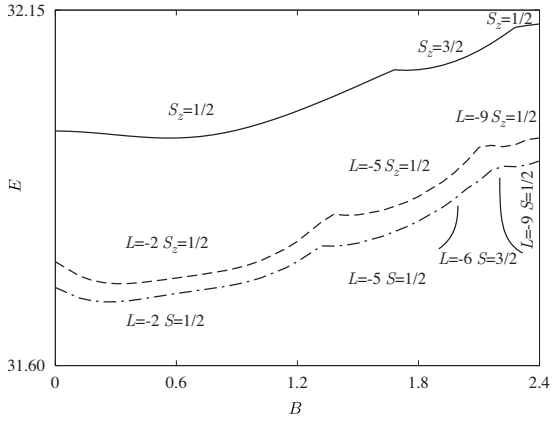

FIG. 8. Ground state energy E (units ω_0) as a function of magnetic field B (units T) for $N=7$. Solid: UHF; dashed: angular momentum projection; dashed dotted: PHF.

Most interesting is $N=7$ (Fig. 8): near $B\approx 2.2$ T the ground state has $S=3/2$. This can only be obtained including the spin projection and leads eventually to a spin blockade in the transport (see below).

In Fig. 9, we show the scheme of the ground state quantum numbers for $4\leqslant N\leqslant 7$, as obtained by PHF. They qualitatively agree with previous calculations,[62,84] performed for $N\leqslant 6$. In the region of B, where the ground state of $N=7$ has $S=3/2$, the state with $N=6$ is a singlet. Since $\Delta S>1/2$ between the two ground states, a spin blockade in the $6\leftrightarrows 7$ transition can be expected near the edge of $\nu=2$ for $N=7$ electrons for $B\approx 2.3$ T. We note in passing that the lowest excited states for $N=7$, with $L=-5$, $S=1/2$ and $L=-9$, $S=1/2$, are at most ≈ 0.07 meV (≈ 0.8 mK) higher in energy. Thus, it may be hard to experimentally observe this blockade.

The chemical potential traces $\mu_N(B)=E_{\mathrm{PHF}}(N,B)-E_{\mathrm{PHF}}(N-1,B)$ obtained by PHF when varying B are experimentally accessible via Coulomb blockade. Figure 10 shows $\mu_5(B)$, $\mu_6(B)$, and $\mu_7(B)$. Arrows indicate the onset of $\nu=2$ for the configuration with $N=5$ (bottom panel), $N=6$ (center), $N=7$ (top). The chemical potentials exhibit features related to the above discussed crossovers between ground states. At the onset of $\nu=2$, the chemical potentials exhibit a cusp. For even N, this corresponds to the above mentioned singlet-triplet transition.[30] Generally, the chemical potentials show kinks when quantum numbers of the ground states change (Figs. 9 and 10).

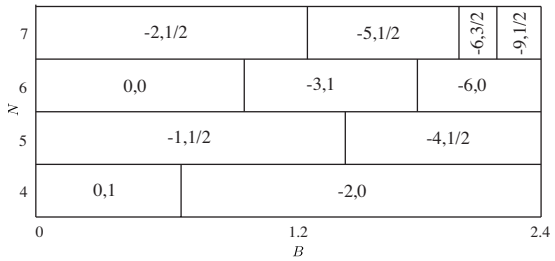

FIG. 9. Scheme of the quantum numbers L,S of the PHF ground state as a function of the magnetic field B (units T) for $4\leqslant N\leqslant 7$.

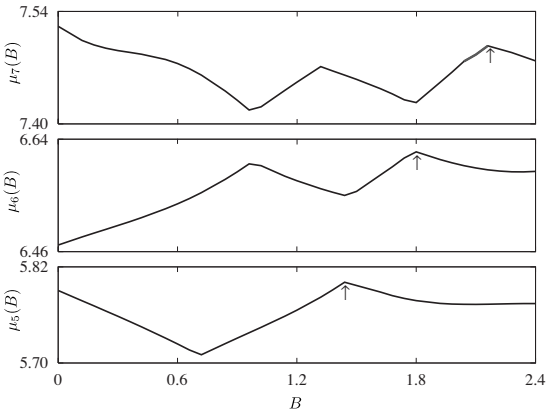

FIG. 10. Chemical potentials $\mu_5(B)$, $\mu_6(B)$, and $\mu_7(B)$ (units ω_0) as a function of B (unit T). Arrows: edge of filling factor $\nu=2$ for $N=5$ (bottom panel), $N=6$ (center), and $N=7$ (top). Red line: region of intrinsic spin blockade (see text).

IV. CONCLUSION

We have described a systematic procedure to overcome some of the limitations of UHF approach. Using angular momentum *and* total spin projections, we have introduced correlations that provide lower estimates for the ground state energies, besides determining the spin and the angular momentum. Several sources of errors have been discussed. In particular, a degeneracy error has been found to be useful for deciding whether or not the estimate for the ground state is plausible.

The procedure yields results consistent with earlier findings for interaction strengths $\lambda\lesssim 2$ which corresponds to experimentally relevant confinement energies $\omega_0\gtrsim 3$ meV for $\varepsilon_r=12.4$.[9,11]

For $B=0$ and $\lambda\leqslant 2$, we have confirmed Hund's first rule for the dot total spin, except for $N=10$. In this case, the ground state is ambiguous, since the energy gap between ground and first excited state is smaller than the degeneracy error. For stronger interaction, $\lambda>4$, deviations from Hund's rules are obtained, with ground states with zero angular momentum and high spin. These may signal the early occurrence of rigid rotating Wigner molecules in PHF solutions.

We have shown that PHF predicts correctly the features of the ground state energy as a function of B. We have found a spin blockade in the transport between $N=6$ and $N=7$, occurring at a filling factor $\nu\approx 2$.

Given the slower increase in computational effort with particle number described in Sec. II C, as compared to other methods, we hope by parallelization of our code to obtain in the future results for higher number of particles ($N\geqslant 20$), varying B, for interaction strengths relevant to quantum dot experiments, $\lambda\leqslant 2$.

That the densities are correctly reproduced suggests that tunneling rates between the quantum dot and attached leads needed for electron transport can be reasonably well estimated when using PHF wave functions. This might be useful for providing quantitative results for predicting the heights of the Coulomb blockade peaks as a function of B.[16,20,22,23]

ACKNOWLEDGMENTS

This work has been supported by the Italian MIUR via No. PRIN05, by the European Union via Contract No. MRTN-CT-2003-504574, and by No. SFB 508 "Quantenmaterialien" of the Universität Hamburg.

APPENDIX: PROJECTION TECHNIQUE

We provide some technical details about the implementation of the projection technique outlined in Sec. II C, in order to obtain Eq. (12). Here, we avoid explicit reference to electron coordinates unless when strictly necessary.

For evaluating $|T_q\rangle=\Sigma_{i=1}^{n_q}|T_q^{(i)}\rangle$, we need to generate all the n_q swaps of q opposite spin pairs in $|T_0\rangle$. This correspond to a special class of permutations, acting on the kth component of the generalized vector,

$$\boldsymbol{\sigma}=(\chi^+,\ldots,\chi^+,\chi^-,\ldots,\chi^-), \tag{A1}$$

with the correspondence $k\rightarrow\pi_k^{(q,i)}$. One then has

$$|T_q\rangle=\frac{1}{\sqrt{N!}}\sum_{i=1}^{n_q}\det\{w_1\sigma_{\pi_1^{(q,i)}},\ldots,w_N\sigma_{\pi_N^{(q,i)}}\}, \tag{A2}$$

with $\mathbf{w}=(u_1^+,\ldots,u_{N_+}^+,u_1^-,\ldots,u_{N_-}^-)$. All the permutations are pretabulated at the beginning of the calculation. Further calculations are performed by means of well-known theorems[41] for many-body wave functions. For the overlap terms, one needs to evaluate[50]

$$\langle T_0|T_q^{(i)}(\gamma)\rangle=\det\{d^{(q,i)}(\gamma)\}, \tag{A3}$$

where $d^{(q,i)}$ is the overlap matrix

$$d_{k_1k_2}^{(q,i)}(\gamma)=\langle w_{k_1}|w_{k_2}(\gamma)\rangle\langle\sigma_{k_1}|\sigma_{\pi_{k_2}^{(q,i)}}\rangle. \tag{A4}$$

Here, $1\leqslant k_1,\ k_2\leqslant N$ and $w_{k_2}(\gamma)=w_{k_2}(r,\vartheta+\gamma)$. The term $\langle\sigma_{k_1}|\sigma_{\pi_{k_2}^{(q,i)}}\rangle$ reduces to a Kronecker delta. For the evaluation of $\langle w_{k_1}|w_{k_2}(\gamma)\rangle$, we use the FD basis. The spatial parts transform as

$$w_{k_2}(\gamma)=\sum_{\mu=1}^{K}C_{\mu i}^{\alpha_{k_2}}e^{il_\mu\gamma}\phi_\mu(r,\vartheta), \tag{A5}$$

with l_μ the angular momentum of the μth FD state, $\alpha_{k_2}=+$ for $p\leqslant N_+$, and $\alpha_{k_2}=-$ for $N_++1\leqslant k_2\leqslant N$. Therefore,

$$\langle w_{k_1}|w_{k_2}(\gamma)\rangle=\sum_{\mu=1}^{K}(C_{\mu k_1}^{\alpha_{k_1}})^*C_{\mu k_2}^{\alpha_{k_2}}e^{il_\mu\gamma}. \tag{A6}$$

The term H_0 in the Hamiltonian ($H=H_0+V$) is

$$\langle T_0|H_0|T_q^{(i)}(\gamma)\rangle=\sum_{k_j=1}^{N}h_{0,k_1k_2}^{(q,i)}(\gamma)D_{k_1|k_2}^{(q,i)}(\gamma), \tag{A7}$$

with $D_{k_1|k_2}^{(q,i)}(\gamma)$ the k_1,k_2 first order cofactor of $d^{(q,i)}$, and

$$h_{0,k_1k_2}^{(q,i)}(\gamma)=\langle w_{k_1},\sigma_{k_1}|h_0|w_{k_2}(\gamma),\sigma_{\pi_p^{(q,i)}}\rangle. \tag{A8}$$

In the interaction part,

$$\langle T_0|V|T_q^{(i)}(\gamma)\rangle=\frac{1}{2}\sum_{k_j=1}^{N}\langle w_{k_1}w_{k_2}|v|w_{k_3}(\gamma)w_{k_4}(\gamma)\rangle\langle\sigma_{k_1}|\sigma_{\pi_{k_3}^{(q,i)}}\rangle\times\langle\sigma_{k_2}|\sigma_{\pi_{k_4}^{(q,i)}}\rangle D_{k_1k_2|k_3k_4}^{(q,i)}(\gamma), \tag{A9}$$

where $D_{k_1k_2|k_3k_4}^{(q,i)}(\gamma)$ represents the second order cofactor of the matrix $d^{(q,i)}(\gamma)$. Terms $H_{0,k_1k_2}^{(q,i)}(\gamma)$ and $V_{k_1k_2k_3k_4}^{(q,i)}(\gamma)$ are evaluated as for Eq. (A6).

[1] See, e.g., S. M. Reimann and M. Manninen, Rev. Mod. Phys. **74**, 1283 (2002); M. Manninen and S. M. Reimann, arXiv:cond-mat/0703292 (unpublished), and references therein.

[2] P. A. Maksym, Phys. Rev. B **53**, 10871 (1996).

[3] C. Yannouleas and U. Landman, Phys. Rev. Lett. **82**, 5325 (1999); **85**, 2220 (2000).

[4] C. Yannouleas and U. Landman, Phys. Rev. Lett. **85**, 1726 (2000).

[5] S. A. Mikhailov, Phys. Rev. B **65**, 115312 (2002).

[6] I. Romanovsky, C. Yannouleas, and U. Landman, Phys. Rev. Lett. **93**, 230405 (2004); L. O. Baksmaty, C. Yannouleas, and U. Landman, Phys. Rev. A **75**, 023620 (2007).

[7] A. Bohr and B. R. Mottelson, *Nuclear Structure* (W. A. Benjamin, London, 1975).

[8] W. de Heer, Rev. Mod. Phys. **65**, 611 (1993).

[9] L. P. Kouwenhoven, C. M. Marcus, P. L. McEuen, S. Tarucha, R. M. Westervelt, and N. S. Wingreen, in *Electron transport in quantum dots*, NATO Advanced Studies Institute, Series E: Applied Science, edited by L. L. Sohn, L. P. Kouwenhoven, and G. Schön (Kluwer, Dordrecht, 1997), p. 105.

[10] L. P. Kouwenhoven, T. H. Oosterkamp, M. W. S. Danoesastro, M. Eto, D. G. Austing, T. Honda, and S. Tarucha, Science **278**, 1788 (1997).

[11] S. Tarucha, D. G. Austing, T. Honda, R. J. van der Hage, and L. P. Kouwenhoven, Phys. Rev. Lett. **77**, 3613 (1996); S. Sasaki, D. G. Austing, and S. Tarucha, Physica B **256**, 157 (1998).

[12] R. Hanson, L. P. Kouwenhoven, J. R. Petta, S. Tarucha, and L. M. K. Vandersypen, Rev. Mod. Phys. **79**, 1217 (2007).

[13] D. Weinmann, W. Häusler, and B. Kramer, Phys. Rev. Lett. **74**, 984 (1995).

[14] A. K. Huettel, H. Qin, A. W. Holleitner, R. H. Blick, K. Neumaier, D. Weinmann, K. Eberl, and J. P. Kotthaus, Europhys. Lett. **62**, 712 (2003).

[15] F. Cavaliere, A. Braggio, J. T. Stockburger, M. Sassetti, and B. Kramer, Phys. Rev. Lett. **93**, 036803 (2004); F. Cavaliere, A. Braggio, M. Sassetti, and B. Kramer, Phys. Rev. B **70**, 125323 (2004).

[16] M. C. Rogge, F. Cavaliere, M. Sassetti, R. J. Haug, and B. Kramer, New J. Phys. **8**, 298 (2006).

[17] M. Ciorga, M. Pioro-Ladriere, P. Zawadzki, P. Hawrylak, and A. S. Sachrajda, Appl. Phys. Lett. **80**, 2177 (2002).

[18] B. Muralidharan and S. Datta, Phys. Rev. B **76**, 035432 (2007).

[19] M. C. Rogge, C. Fuhner, U. F. Keyser, and R. J. Haug, Appl. Phys. Lett. **85**, 606 (2004).

[20] M. Ciorga, A. Wensauer, M. Pioro-Ladriere, M. Korkusinski, J. Kyriakidis, A. S. Sachrajda, and P. Hawrylak, Phys. Rev. Lett. **88**, 256804 (2002).
[21] M. Ciorga, A. S. Sachrajda, P. Hawrylak, C. Gould, P. Zawadzki, S. Jullian, Y. Feng, and Z. Wasilewski, Phys. Rev. B **61**, R16315 (2000).
[22] D. Kupidura, M. C. Rogge, M. Reinwald, W. Wegscheider, and R. J. Haug, Phys. Rev. Lett. **96**, 046802 (2006).
[23] M. C. Rogge, C. Fühner, and R. J. Haug, Phys. Rev. Lett. **97**, 176801 (2006).
[24] M. Stopa, W. G. van der Wiel, S. De Franceschi, S. Tarucha, and L. P. Kouwenhoven, Phys. Rev. Lett. **91**, 046601 (2003).
[25] M. Keller, U. Wilhelm, J. Schmid, J. Weis, K. v. Klitzing, and K. Eberl, Phys. Rev. B **64**, 033302 (2001).
[26] B. Reusch, W. Häusler, and H. Grabert, Phys. Rev. B **63**, 113313 (2001).
[27] B. Reusch and H. Grabert, Phys. Rev. B **68**, 045309 (2003).
[28] B. Szafran, S. Bednarek, J. Adamowski, M. B. Tavernier, E. Anisimovas, and F. M. Peeters, Eur. Phys. J. D **28**, 373 (2004).
[29] A. Emperador, E. Lipparini, and Ll. Serra, Phys. Rev. B **73**, 235341 (2006).
[30] A. Wensauer, M. Korkusinski, and P. Hawrylak, Phys. Rev. B **67**, 035325 (2003).
[31] P. Hawrylak, C. Gould, A. Sachrajda, Y. Feng, and Z. Wasilewski, Phys. Rev. B **59**, 2801 (1999).
[32] M. Koskinen, M. Manninen, and S. M. Reimann, Phys. Rev. Lett. **79**, 1389 (1997).
[33] K. Hirose and N. S. Wingreen, Phys. Rev. B **59**, 4604 (1999).
[34] M. Gattobigio, P. Capuzzi, M. Polini, R. Asgari, and M. P. Tosi, Phys. Rev. B **72**, 045306 (2005).
[35] A. Harju, H. Saarikoski, and E. Räsänen, Phys. Rev. Lett. **96**, 126805 (2006).
[36] E. Räsänen, J. Konemann, R. J. Haug, M. J. Puska, and R. M. Nieminen, Phys. Rev. B **70**, 115308 (2004).
[37] H. Saarikoski, E. Räsänen, S. Siljamäki, A. Harju, M. J. Puska, and R. M. Nieminen, Phys. Rev. B **67**, 205327 (2003).
[38] N. Helbig, S. Kurth, S. Pittalis, E. Räsänen, and E. K. U. Gross, arXiv:cond-mat/0605599 (unpublished).
[39] A. Szabo and N. S. Ostlund, *Modern Quantum Chemistry* (Dover, New York, 1999).
[40] P.-O. Löwdin, Phys. Rev. **97**, 1509 (1955).
[41] P.-O. Löwdin, Phys. Rev. **97**, 1474 (1955).
[42] P. Ring and P. Schuck, *The Nuclear Many-Body Problem* (Springer-Verlag, New York, 1980).
[43] C. Yannouleas and U. Landman, Phys. Rev. B **68**, 035325 (2003).
[44] C. Yannouleas and U. Landman, Phys. Rev. B **69**, 113306 (2004).
[45] Y. Li, C. Yannouleas, and U. Landman, Phys. Rev. B **73**, 075301 (2006).
[46] H.-M. Müller and S. E. Koonin, Phys. Rev. B **54**, 14532 (1996).
[47] C. Yannouleas and U. Landman, J. Phys.: Condens. Matter **14**, L591 (2002).
[48] C. Yannouleas and U. Landman, Eur. Phys. J. D **16**, 373 (2001).
[49] C. Yannouleas and U. Landman, Int. J. Quantum Chem. **90**, 699 (2002).
[50] U. D. Giovannini, F. Cavaliere, R. Cenni, M. Sassetti, and B. Kramer, New J. Phys. **9**, 93 (2007).
[51] Ll. Serra, R. G. Nazmitdinov, and A. Puente, Phys. Rev. B **68**, 035341 (2003).
[52] A. Puente, L. Serra, and R. G. Nazmitdinov, Phys. Rev. B **69**, 125315 (2004).
[53] M. Dineykhan and R. G. Nazmitdinov, Phys. Rev. B **55**, 13707 (1997).
[54] D. Pfannkuche, V. Gudmundsson, and P. A. Maksym, Phys. Rev. B **47**, 2244 (1993).
[55] M. Wagner, U. Merkt, and A. V. Chaplik, Phys. Rev. B **45**, 1951 (1992).
[56] S. A. Mikhailov and N. A. Savostianova, Phys. Rev. B **66**, 033307 (2002).
[57] S. A. Mikhailov, Phys. Rev. B **66**, 153313 (2002).
[58] P. Hawrylak and D. Pfannkuche, Phys. Rev. Lett. **70**, 485 (1993).
[59] P. Hawrylak, Phys. Rev. Lett. **71**, 3347 (1993).
[60] A. Wojs and P. Hawrylak, Phys. Rev. B **53**, 10841 (1996).
[61] M. B. Tavernier, E. Anisimovas, F. M. Peeters, B. Szafran, J. Adamowski, and S. Bednarek, Phys. Rev. B **68**, 205305 (2003).
[62] H. Imamura, H. Aoki, and P. A. Maksym, Phys. Rev. B **57**, R4257 (1998).
[63] J. Kyriakidis and C. J. Stevenson, arXiv:cond-mat/0608044 (unpublished).
[64] Y. Nishi, P. A. Maksym, D. G. Austing, T. Hatano, L. P. Kouwenhoven, H. Aoki, and S. Tarucha, Phys. Rev. B **74**, 033306 (2006).
[65] A. Wensauer, M. Korkusinski, and P. Hawrylak, Solid State Commun. **130**, 115 (2004).
[66] M. Rontani, C. Cavazzoni, D. Bellucci, and G. Goldoni, J. Chem. Phys. **124**, 124102 (2006).
[67] K. Varga, P. Navratil, J. Usukura, and Y. Suzuki, Phys. Rev. B **63**, 205308 (2001).
[68] F. Pederiva, C. J. Umrigar, and E. Lipparini, Phys. Rev. B **62**, 8120 (2000); **68**, 089901(E) (2003).
[69] L. Colletti, F. Pederiva, E. Lipparini, and C. J. Umrigar, Eur. Phys. J. B **27**, 385 (2002).
[70] R. Egger, W. Häusler, C. H. Mak, and H. Grabert, Phys. Rev. Lett. **82**, 3320 (1999); **83**, 462 (1999).
[71] A. Harju, S. Siljamäki, and R. M. Nieminen, Phys. Rev. B **65**, 075309 (2002).
[72] F. Bolton, Phys. Rev. B **54**, 4780 (1996).
[73] A. Ghosal, A. D. Güçlü, C. J. Umrigar, D. Ullmo, and H. U. Baranger, Nat. Phys. **2**, 336 (2006).
[74] A. Ghosal, A. D. Güçlü, C. J. Umrigar, D. Ullmo, and H. U. Baranger, Phys. Rev. B **76**, 085341 (2007).
[75] A. D. Güçlü, A. Ghosal, C. J. Umrigar, and H. U. Baranger, arXiv:0708.1304 (unpublished).
[76] E. Räsänen, H. Saarikoski, A. Harju, M. Ciorga, and A. Sachrajda (unpublished).
[77] W. Y. Ruan, Y. Y. Liu, C. G. Bao, and Z. Q. Zhang, Phys. Rev. B **51**, 7942 (1995).
[78] A. V. Filinov, M. Bonitz, and Yu. E. Lozovik, Phys. Rev. Lett. **86**, 3851 (2001).
[79] Chengguang Bao, Wenying Ruan, and Youyang Liu, Phys. Rev. B **53**, 10820 (1996).
[80] V. Fock, Z. Phys. **47**, 446 (1928); G. C. Darwin, Proc. Cambridge Philos. Soc. **27**, 86 (1930).
[81] V. H. Smith, J. Chem. Phys. **41**, 277 (1964).
[82] M. B. Ruiz, J. Math. Chem. **24**, 233 (1998).
[83] M. Rontani, C. Cavazzoni, and G. Goldoni, Comput. Phys. Commun. **169**, 430 (2005).
[84] M. B. Tavernier, E. Anisimovas, and F. M. Peeters, Phys. Rev. B **74**, 125305 (2006).
[85] S. Tarucha, D. G. Austing, Y. Tokura, W. G. van der Wiel, and L. P. Kouwenhoven, Phys. Rev. Lett. **84**, 2485 (2000).